Received November 15, 2020, accepted December 1, 2020, date of publication December 7, 2020,
date of current version December 28, 2020.

Digital Object Identifier 10.1109/ACCESS.2020.3043003

Parallel Computing for Obtaining Regional Scale Rice Growth Conditions Based on WOFOST and Satellite Images

BINGYU ZHAO[1], MEILING LIU[2], JIANJUN WU[1,3,4], XIANGNAN LIU[2], MENGXUE LIU[1,5,6], AND LING WU[2]

[1]Faculty of Geographical Science, Beijing Normal University, Beijing 100875, China
[2]School of Information Engineering, China University of Geosciences, Beijing 100083, China
[3]State Key Laboratory of Remote Sensing Science, Beijing Normal University, Beijing 100875, China
[4]Beijing Key Laboratory for Remote Sensing of Environment and Digital Cites, Beijing Normal University, Beijing 100875, China
[5]State Key Laboratory of Earth Surface Processes and Resource Ecology, Beijing Normal University, Beijing 100875, China
[6]College of Resources Science and Technology, Beijing Normal University, Beijing 100875, China

Corresponding author: Jianjun Wu (jjwu@bnu.edu.cn)

This work was supported in part by the National Key Research and Development Program of China under Grant 2017YFC1502402; and in part by the National Natural Science Foundation of China under Grant 41671424, Grant 42071391, Grant 41371407, and Grant 41701387.

ABSTRACT It is very important to obtain continuous regional crop parameters efficiently in the agricultural field. However, remote sensing data can provide spatial-continuous / temporal-disperse crop information while crop growth model can provide temporal-continuous / spatial-disperse crop information. Therefore, the assimilation between crop growth model and remote sensing data is an efficient way for obtaining continuous vegetation growth information. This study aims to present a parallel method based on graphic processing unit (GPU) to improve the efficiency of the assimilation between RS data and crop growth model to estimate rice growth parameters. Remote sensing data, Landsat and HJ-1 images, were collected and the World Food Studies (WOFOST) crop growth model which has a strong flexibility was employed. To acquire continuous regional crop parameters, particle swarm optimization (PSO) data assimilation method was used to combine remote sensing images and WOFOST and this process is accompanied by a parallel method based on the Compute Unified Device Architecture (CUDA) platform of NVIDIA GPU. With these methods, we obtained daily rice growth parameters of Zhuzhou City, Hunan, China and compared the efficiency and precision of parallel method and non-parallel method. Results showed that the parallel program has a remarkable speedup (reaching 240 times) compared with the non-parallel program with a similar accuracy. This study indicated that the parallel implementation based on GPU was successful in improving the efficiency of the assimilation between RS data and the WOFOST model.

INDEX TERMS WOFOST model, data assimilation, remote sensing, parallel algorithm.

I. INTRODUCTION

Data assimilation, which is of momentous theoretical and application values, has been successfully applied to numerous fields, such as atmosphere [1]–[3], weather [4]–[6], agriculture [7]–[9], ocean [10]–[12], land surface [13]–[15] and hydrology [16]–[18]. Assimilating remote sensing (RS) information into a crop model can provide continuous regional plant growth information and has been applied to a wide range of agricultural fields in crop growth assessment, agricultural environmental control and farmland management decision [19]–[23].

The assimilation between RS data and crop growth model regards RS information (continuous in spatial scale and discrete in time scale) as the measured variables. In addition, the model's simulating process is optimized with an assimilation algorithm to obtain vegetation information successive in spatial and temporal scales [24]. On the basis of various RS data, crop growth models and assimilation algorithms, researchers have conducted numerous studies on the different applications of assimilating RS information into crop models [20], [22], [25]–[27]. Huang [28] conducted

The associate editor coordinating the review of this manuscript and approving it for publication was Wenming Cao.

an experiment on regional winter wheat yield forecasting with moderate-resolution imaging spectroradiometer-leaf area index (MODIS-LAI) products on the basis of assimilation between the World Food Studies (WOFOST) model [29]–[32] and ensemble Kalman algorithm method [33]–[36]. Their results indicated a remarkable improvement compared with statistical yield, which provides a reliable approach for predicting regional crop yield. Jin *et al.* [37] developed an improved assimilation method with Landsat 8 images on the basis of the WOFOST model and particle swarm optimization (PSO) algorithm [38]–[42] for the efficient assessment of heavy metal stress levels in rice.

Previous studies on the assimilation of the crop growth model and RS data often focus on its precision but not on its efficiency. However, when the study scale expands, current methods for assimilation cannot satisfy the needs for rapidly obtaining continuous accurate crop growth information in a large scale. The first need involves the tremendous amounts of data in the assimilation. RS images reflect vast earth surface information and their data volume is often large. With the improvement of the image's spatial and temporal resolution and the extension of the study area, the number of pixels to assimilate will increase quickly and the calculation volume will be enormous. The second need includes computationally expensive algorithms. The crop growth model quantificationally simulates the complex growth processes, such as the crop development process, CO2 assimilation, respiration and leaf area simulation [43]–[47]. In addition, the assimilation algorithms generally require considerable iterations to optimize the model's simulating process and must conduct a series of calculations in each iteration [48].

In recent years, graphic processing unit (GPU)-based high-performance computing technology has been increasingly applied in large-scale computing scenarios, such as mathematical calculations, image processing, computational biology and chemistry and fluid dynamics simulation [49]–[55]. Early works on GPU-based processing for RS data have been conducted by numerous researchers [56]–[62]. Wei and Huang [63] explored a GPU-based implementation of the extended Kalman filter. The Compute Unified Device Architecture (CUDA) on the Nvidia GeForce GTX 590 GPU was used. The speedup reached 1386x and the parallel implementation of extended Kalman filter will serve as good reference on real large-scale applications. Blattner and Yang [64] utilized the CUDA programming framework in numerical weather prediction by the data assimilation method, local ensemble transformed Kalman filter algorithm. Results show that an improvement of 72.1× speedup and provide attractive evidence for applying CUDA GPUs to high demanding scientific computation realms. Zheng *et al.* [65] first use GPU and CUDA technology on RRTM (Rapid Radiative transfer module) long-wave radiation module of GRAPES (Global and Regional Assimilation and Prediction System) model for parallel processing. The results show that the parallel computing algorithm is correct, stable and efficient for operational implementation of GRAPES in near future. The assimilation calculations for each rice pixel on the RS image are not only consistent but also mutually independent; thus, the parallel implementation is feasible.

In this study, we develop a highly efficient GPU-based parallel program for the assimilation of the WOFOST model and RS images with the PSO algorithm on the CUDA platform. We input the most time-consuming work (each rice pixel's assimilation with the WOFOST model) to a specific thread on the GPU and concurrently execute all threads. The execution time and assimilating precision of serial and parallel programs are compared. With the parallel assimilating results, we simulate the spatial distribution of three important rice growth parameters, LAI, root weight (WRT) and panicle weight (WSO), on a large scale.

II. STUDY AREA AND DATA

A. STUDY AREA

The main study region (112°17'-114°07' E, 26°03'-28°01' N) is located in Zhuzhou City, Hunan, China, with an entire area of approximately 1836.28 m^2 (Figure 1). This area has a subtropical monsoon humid climate with adequate illumination, annual average temperature of 15.5-25°C and annual precipitation of 1250–1500 mm, which is suitable for crop growth. Zhuzhou City is an important food base and its grain output is higher than those of other regions in Hunan Province. Fast and accurate monitoring of crop growth information in this region is important.

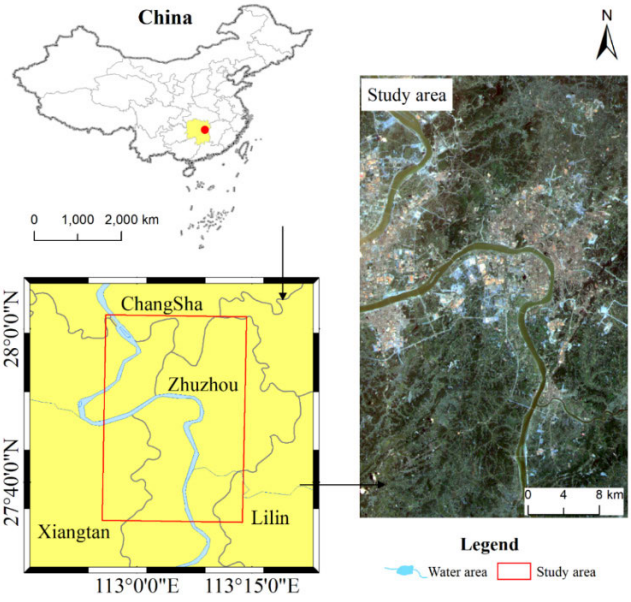

FIGURE 1. Location of the study area in Hunan Province, China.

B. DATA PREPARATION

The main data of this work contain two parts: RS data for deriving measured assimilating observations and meteorological data for external input data of the WOFOST model. In this study, Landsat 7 (Enhanced Thematic Mapper Plus (ETM+) sensor) and HJ-1A/B (charge-coupled device (CCD)) satellite imagery were jointly used to generate

TABLE 1. Landsat and HJ-1A/B images used in this study.

Year	2015	2016	2017
DOY	194* 210* 216 259	205 212 233 258	203 215* 232 261

* represents the Landsat images; Rest are the HJ-1A/B images. DOY represents the day of the year.

measured LAI (MLAI) series [66]. Table 1 shows the parameters of these images. Radiometric calibration and atmospheric correction were conducted for these two types of images. The radiometric calibration for CCD images was based on the absolute radiation calibration coefficient of HJ-1A/B, released by the China Resources Satellite Application Center. In addition, the Fast Line-of-sight Atmospheric Analysis of Spectral Hypercubes model was adopted for the atmospheric correction of all images. The corrected root-mean-square error was less than 0.5 pixels. All images were downloaded from the United States Geological Survey (http://glovis.usgs.gov/) and China Centre for Resources Satellite Data and Application (http://www.cresda.com). The meteorological data included the daily maximum air temperature (TMAX), daily minimum air temperature (TMIN) and daily solar radiation (AVRAD) from June 1 to September 30 in 2015, 2016 and 2017. They are obtained from China Meteorological Data Sharing Service System. As the spatial scale of the study area is not too big, according to the law of Geographic Similarity, it is reasonable to use the data from one meteorological station (Zhuzhou Station) to represent the meteorological factors of the whole study area.

In this work, we select LAI as the assimilative observation because it is an important index that reflects the growth status of plant population and a primary output result of the WOFOST model. The measured rice LAI series are calculated with RS images. In this study, we extract rice region in the study area with a random forest algorithm [67]–[70] and then calculate rice LAI through its NDVI obtained from RS images. Previous studies have shown that the exponential empirical model between LAI and NDVI in this area is practicable and most widely used [71]. The empirical model was established by using the local measured LAI data and NDVI conversion index in Zhuzhou City. And its R2 is 0.84 and the MSE is 0.06, which is acceptable in the actual data assimilation process. Their transformational relationship is expressed in the following equation:

$$LAI = 0.361 \times e^{3.69 \times NDVI} \quad (1)$$

Then, we can obtain the MLAI series. We extract a total of 401296 rice pixels with a valid LAI in the study area.

III. METHODS

Figure 2 shows the overall technical roadmap of this work. The parallel implementation of the assimilation between

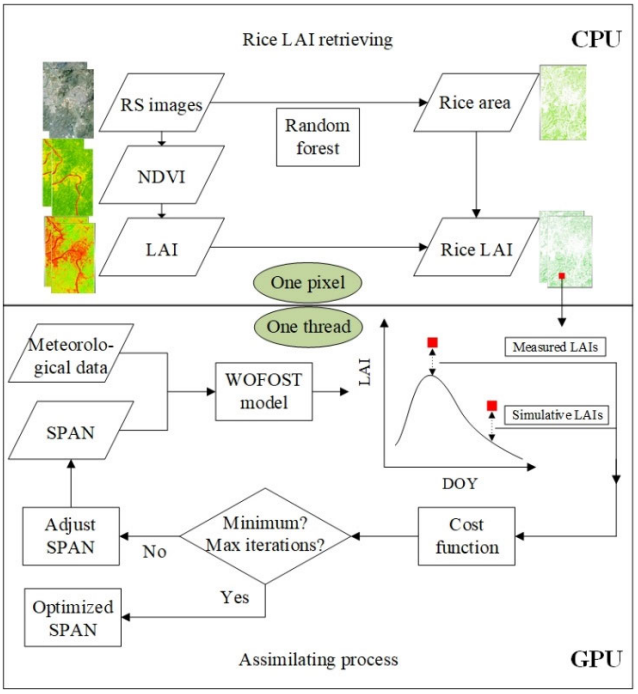

FIGURE 2. General flow chart for estimating rice growth parameters based on the GPU.

RS images and the WOFOST model with the PSO algorithm mainly includes two parts: retrieving MLAI from RS images in the Environment for Visualising Images (ENVI) on the CPU and assimilating all rice pixels' MLAI with the simulative LAI (SLAI) series calculated from the WOFOST model synchronously on the GPU. The lower part of Figure 2 presents each rice pixel's assimilating process, i.e. each thread's computational task. Each thread's output result is an optimised leaf senescence index, which is an input parameter of the WOFOST model.

A. ASSIMILATION BETWEEN THE WOFOST MODEL AND RS DATA

Each thread's computational task includes each rice pixel's assimilation between SLAI calculated from the WOFOST model and MLAI retrieved from RS data, which is the most time-consuming in the assimilating process. The methods for obtaining MLAI from satellite images are previously discussed. The methods for obtaining SLAI from the WOFOST model and assimilation are presented as follows.

The assimilation between the WOFOST model and RS data involves obtaining the model's optimal input parameters for each rice pixel on the RS image through the assimilation algorithm. The input parameters to be optimised must satisfy two conditions: (1) difficult to obtain in a regional scale and (2) closely related to the output results of WOFOST. Considering these principles, we selected SPAN as the input parameter to be optimised. SPAN (day) is the leaf senescence index, which refers to the life cycle of leaves at 35 °C. Generally, SPAN ranges from 17 to 50 [72]. As the exact

value of SPAN for each pixel is difficult to determine due to the individual differences of rice [73], we select a random value in its range as the initial input of the WOFOST model. The meteorological data and initial randomised SPAN are the input data of the WOFOST model, and the output result is an interannual LAI series at the time step of 1 day. Then, we can extract the SLAI at the acquisition time of images. In this study, the meteorological data from one weather station is used to represent the entire study area, because the area of this study is relatively small. The crop data in the WOFOST model includes: specific leaf area, net photosynthetic rate, dry matter distribution coefficient, etc. Since the research object of this article is rice, the rice varieties in this area are relatively uniform, so uniform crop parameters are used in this study area.

However, a certain error occurs between SLAI and MLAI. The PSO algorithm will reduce this error by adjusting SPAN through considerable iterations. In the PSO algorithm, the error is calculated as follows:

$$C = \sqrt{\frac{1}{N}\sum_{i=1}^{N}(LAI_m - LAI_s)^2} \quad (2)$$

where N is the number of RS images in a year; LAI_m and LAI_s denote the MLAI and SLAI, respectively; and C represents the degree of deviation between LAIm and LAIs. When C reaches its minimal mean, the SLAI series are closest to the actual LAI, and the corresponding SPAN is optimised.

Finally, each rice pixel's daily growth parameters are calculated with the rectified WOFOST model (the optimum SPAN as its input parameter). Then, we can continuously analyse the rice growth information on a regional scale.

B. NVIDIA GPU ARCHITECTURE

We have utilized the Pascal architecture-based GPU (Tesla P40) with CUDA to realize the parallel implementation of the assimilating process. A brief introduction of the Pascal architecture and CUDA program model is presented as follows.

1) PASCAL ARCHITECTURE

The GPU architecture is constructed by using extensible arrays with a streaming multiprocessor (SM). The hardware is parallelized on the GPU by copying the SM. The Pascal architecture produced by NVIDIA in 2016 is a quick, efficient and high-performance computing architecture. Similar to previous Tesla-class GPUs, the Pascal architecture is composed of an array of graphics processing clusters (GPCs), texture processing clusters (TPCs), SMs and memory controllers. A full Pascal architecture consists of six GPCs, 60 Pascal SMs, 20 TPCs (each with two SMs) and eight 512-bit memory controllers. Each GPC has 10 SMs. Each SM has 64 CUDA cores and four texture units. The total number of cores loaded in NVIDIA's Tesla P40 GPU is 3840. Each memory controller is attached to 51 KB of L2 cache [74].

2) CUDA PROGRAMMING MODEL

CUDA is a universal parallel computing platform and programming model and is an extension of the C programming language.

In the CUDA programming model, the CPU is the host terminal, whereas the GPU is the device terminal. Developers can stipulate computation tasks to be parallelized into a kernel function, which is invoked on the host terminal and executed on the device terminal. Before the CPU calls a kernel function, developers have to allocate a memory on the GPU for data sets used in kernels and copy them from the CPU to the GPU. After a kernel finishes, users have to copy the output results from the device to the host [75].

The organization of threads on the GPU is the key for accelerating large-scale data processing. To manage the threads on the GPU further, CUDA has introduced an abstract concept, namely, thread hierarchy. Figure 3 depicts the two levels of thread hierarchy (thread grids and thread blocks [75]. When a kernel is activated, all generating threads form one grid. One grid consists of multiple thread blocks, and one thread block includes a group of threads. The organization of threads involves grouping all threads in one grid. We can artificially set the number of threads in one block and the number of thread blocks in one grid for our program to obtain optimal performance [74].

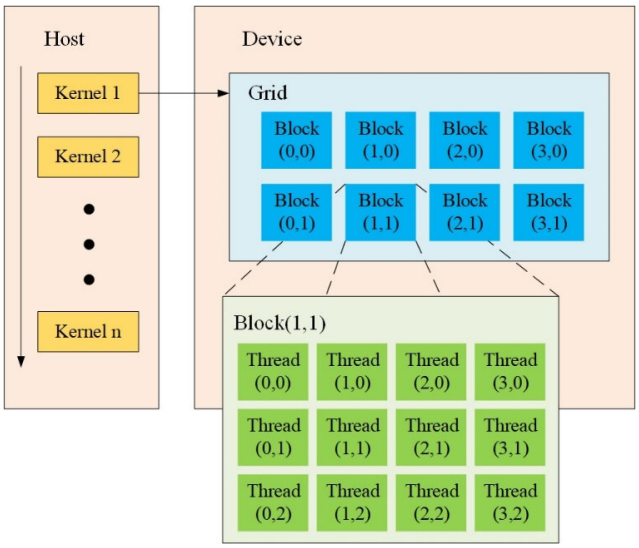

FIGURE 3. GPU's thread hierarchy. Host is the CPU terminal and responsible for serial processes between kernels. Device refers to the GPU terminal, which contains a large number of threads, blocks and grids. Device is in charge of the execution of large-scale parallel computing.

C. PARALLEL IMPLEMENTATION APPROACHES FOR THE ASSIMILATION

In the parallelisation of assimilating RS information into the WOFOST model, NVIDIA Tesla P40 based on Pascal architecture GPU and Xeon E5-2620 CPU is used for the hardware environment. Tesla series is specially designed for large-scale parallel computing. Table 2 presents the technical specifications of P40. The software is developed under

TABLE 2. Technical specification of NVIDIA Tesla P40 GPU.

Compute capability	6.1
Number of cores	3840
Single-precision performance	12 teraflops
Memory capacity	24 GB
Memory bandwidth	346 GB/s

Ubuntu Linux system, and the CUDA codes (.cu) are written in C++ language and compiled with NVCC.

1) THREAD ORGANISATION METHODS ON GPU

MLAI retrieved from satellite images in a year is the main data set and is saved in a 2D array. We assign all rice pixels' LAI values of one image into a 1D vector from top to bottom, from left to right, as one column of MLAI. Moreover, the rice pixels' locations in a 2D image are saved, which will be used in the subsequent simulation of the spatial distribution of rice growth parameters. Thus, the length of MLAI equals the total number of rice pixels in our study area, whereas its width equals the number of RS images obtained in 1 year. Each row represents the MLAI series of one rice pixel. We extract a total of 401296 rice pixels with valid LAI values in the study area, and the length of MLAI is greater than the width. Hence, although the data set is a 2D array, we organize all threads in a 1D manner, and the assimilation for each rice pixel is allocated to a thread (Figure 4). In the kernel function, we can use the thread index to extract the MLAI series of each thread's corresponding rice pixel. As we organized all threads in a 1D manner, the relationship between the index (idx) of one rice pixel's MLAI series and the thread identifiers is as follows:

$$\text{int idx} = \text{threadIdx.x} + \text{blockDim.x} * \text{blockIdx.x}, \quad (3)$$

where threadIdx and blockIdx are the indexes of thread and block, respectively, and blockDim indicates the block size, which is equal to the number of threads in one block.

2) PARALLEL PROGRAM DESIGN

In this work, PSO_WOFOST is set as the kernel function, which indicates that all threads allocated on the GPU will execute the same PSO_WOFOST function with different input data. The prototype is presented as follows:

__global__ void PSO_WOFOST (double *MLAI, double *TMIN, double *TMAX, double *AVRAD, long rand, double *gbest)

PSO_WOFOST is responsible for each rice pixel's assimilating process with the PSO algorithm, i.e. the calculation of optimal SPAN. The main steps of PSO_WOFOST are as follows:

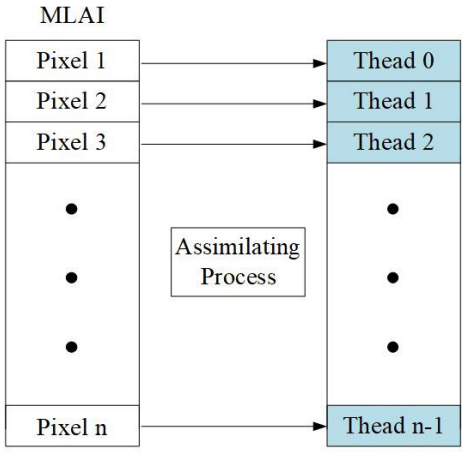

FIGURE 4. Thread organization in a 1D manner. Each row under MLAI stores each rice pixel's MLAI series. N is equal to the total number of rice pixels in our study area. Each rice pixel's assimilating process is allocated to one specific thread on the GPU.

Step 1: Obtain the index of one rice pixel's MLAI series with thread identifiers and extract the rice pixel's MLAI series;

Step 2: Randomly initialize SPAN in its range;

Step 3: Input randomized SPAN and meteorological data into the WOFOST model to calculate SLAI;

Step 4: Calculate the cost function value (C) with SLAI and MLAI through Eq. (2).

Step 5: Assess whether C reaches the minimum. If yes, output the corresponding SPAN to the gbest in accordance with the index in Step 1; if no, adjust SPAN and return to Step 3.

Before kernel function is activated, the data to be transferred from the host terminal to the device terminal include MLAI, TMIN, TMAX and AVRAD. MLAI stores all rice pixels' LAI in a year and TMIN, TMAX and AVRAD store the meteorological data. After the kernel function is finished, all rice pixels' optimal SPAN must be transferred from the GPU to the CPU. gbest stores all rice pixels' SPAN. Transferring such a large data between the GPU and CPU is time-consuming. Thus, to reduce the transferring time, we allocate a pinned memory for the data to be transferred directly instead of a pageable memory on the host terminal. This process will reduce the time of copying data from pageable memory to pinned memory (the GPU can only access the host pinned memory) [74]. We can use the following codes to allocate pinned memory for MLAI.

```
//Allocate pinned memory, nbytes is the size of MLAI
cudaMallocHost ((double **) &MLAI, nbytes);
```

As the methods of memory allocation for variables in the parallel program, the local variables declaring inside the kernel function are located in registers. Given the size of these five datasets are relatively larger and each thread (a pixel's assimilation process) needs to obtain corresponding data from MLAI, TMIN, TMAX AVRAD and assign assimilation result to gbest, we allocated global memory for them in our parallel program.

IV. RESULTS

This section may be divided by subheadings. It should provide a concise and precise description of the experimental results, their interpretation as well as the experimental conclusions that can be drawn.

A. PRECISION ASSESSMENT OF ASSIMILATION IMPLEMENTED ON GPU

We regarded the discrepancy (C) between each rice pixel's MLAI retrieved from satellite imagery and SLAI calculated with the WOFOST model as the standard for measuring the assimilation effect, which is calculated in Eq. (2). We evaluated the assimilation precision in three cases: a) SLAIe, calculated from the WOFOST model that sets experiential SPAN (50) as the input parameter; b) SLAIc, calculated from the WOFOST model that sets the optimized SPAN of the assimilation implemented on the CPU as the input parameter; and c) SLAIg, calculated from the WOFOST model that sets the optimized SPAN of the assimilation implemented on the GPU as the input parameter. However, the comparison of assimilation precision for all rice pixels in our study area is hardly possible to conduct. Thus, we selected six sites within the scope of the study area to compare their assimilation precision. As previously described, we extracted a total of 401296 rice pixels in each RS image and organized them in one dimension. Similarly, the assimilating results, namely, gbest (optimized SPAN for each rice pixel), were stored in one dimension. We divided the gbest equidistantly into six parts and extracted one optimized SPAN in each part. Six optimized SPANs and meteorological data are inputted into the WOFOST model to calculate the SLAIc and SLAIg of the six sites. The results of comparing these six sites' precision represent the assimilation precision of the entire study area. Figure 5 shows the locations of six sites and comparison results of the assimilation precision.

First, SLAI calculated from the WOFOST model that sets the assimilating result (optimized SPAN) as the input parameter is closer to the actual LAI than SLAI calculated from the WOFOST model that sets the experiential SPAN as the input parameter, whether the assimilation is implemented on the GPU or CPU. However, the precision of the assimilation implemented on the GPU is slightly inferior to that on the CPU. The reason is that the GPU is often used for parallel tasks with simple control logic and calculations and poorly handles programs that require high-precision results, whereas the CPU performs better when executing extreme complex programs. Nevertheless, numerous complex floating-point calculations and logical operations in the assimilating process are presented.

B. EVALUATIONS OF GPU PERFORMANCE IN COMPUTATIONAL TIME GAINS

The serial program includes individually executing all rice pixels' assimilation on the CPU, which is the same with the parallel program. However, when the data size

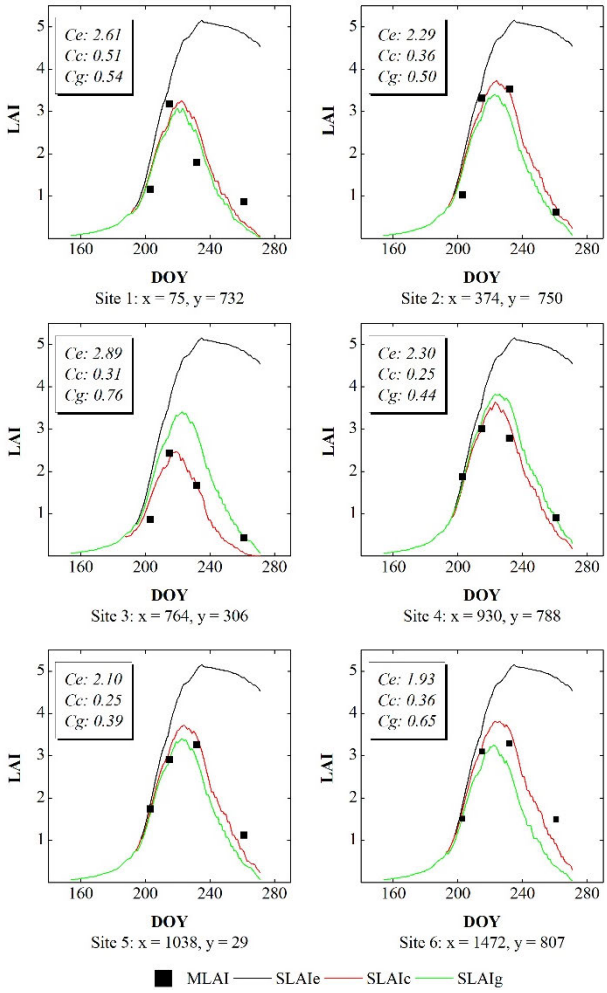

FIGURE 5. Comparison of the assimilation precision of three circumstances. x and y represent the line and column numbers of the sites in the entire study area. Ce, Cc and Cg indicate the MLAI discrepancies with each site's SLAIe, SLAIc and SLAIg, respectively.

(number of rice pixels) is greater than 10000, the memory space on the CPU will be insufficient for storing the variables in the assimilating process. Therefore, we divided all the datasets (401296 pixels) into 41 batches. Each batch size is 10000 and the size of the last one is 1296. When the data size is over 10000, the execution time of different size data sets is the computation time for all batches within the corresponding data set in Table 3.

Table 3 compares the computation times of serial and parallel programs in handling different data sizes (number of rice pixels). Distinctly, the parallel program executed by the GPU for the assimilation considerably outperforms the serial program executed by the CPU. The major reason for the remarkable acceleration is the massive parallelism implemented by a large number of different threads on the GPU that synchronously executes the assimilation processes. However, when the data size is less than 100 pixels, the execution time of the serial program is less than that of the parallel program. This phenomenon results from the frequent memory

TABLE 3. Time consumed by the parallel and serial programs.

Data size (number of rice pixels)	Parallel(s)	Serial(s)	Speedups (×)
1	0.916	0.074	0.081
10	3.982	0.684	0.172
100	4.245	6.612	1.558
1000	6.200	65.907	10.630
10000	17.177	657.855	38.299
100000	51.062	6578.295	128.830
150000	61.349	9867.318	160.839
200000	70.347	13156.424	187.022
250000	78.671	16445.530	209.042
300000	88.771	19734.636	222.309
350000	100.771	23023.742	228.476
400000	109.375	26312.848	240.575
401296	110.059	26398.102	239.854

■ Speedup is defined as the serial execution time divided by the parallel time.

transmission between the GPU and CPU, which can weaken the parallel program's performance. Table 3 shows that the speedup increases with the increase of input data size. The maximum Speedup in this work reaches near 240 times.

C. SPATIAL DISTRIBUTION OF RICE GROWTH PARAMETERS IN A LARGE SCALE

Each rice pixel's optimized SPAN can be used as the input parameter of the WOFOST model to simulate rice LAI daily. WOFOST can also simulate important growth parameters other than LAI, such as WRT and WSO, which can commendably reflect the rice growth conditions. All rice pixels' LAI, WRT and WSO values are reorganized in accordance with the previously saved locations of all rice pixels in the 2D image. As shown in Figure 6, we simulated the spatial distribution of rice LAI, WRT and WSO within the entire study area at several key time nodes during the rice growth season. Figure 7 simulates the dynamic changes of LAI, WRT and WSO at a time step of 5 days during the rice growth season. Generally, LAI, WRT and WSO in 2015 and 2016 are higher than those in 2017, indicating that the rice growth conditions in 2015 and 2016 are better than that in 2017. The speeds of rice growth in 2015 and 2016 are faster than that in 2017, and the speed of rice senescence in 2016 is faster than those in 2015 and 2017. Furthermore, the final WSO in 2016 is higher than those in 2015 and 2017, indicating that the grain output in 2016 is higher than those in 2015 and 2017.

V. DISCUSSION

We mainly improved the efficiency of the assimilation between the WOFOST model and satellite imagery by parallel implementation based on the GPU with CUDA platform. We inputted the most time-consuming work (all rice pixels' assimilation) into thousands of GPU threads and concurrently start all threads to reduce the execution time. We compared the precision and execution times of the assimilation implemented on the CPU and GPU. Although the assimilation precision performance of the GPU is slightly lower than that of the CPU, the gains in the computational time aspect, such as the huge acceleration (240 times) from the GPU's parallel implementation, are sufficiently excellent for application. With the highly efficient parallel assimilating results, we simulated the spatial distribution of rice growth conditions in a large scale.

A comparison with other GPU-based image processing works shows differences in two main aspects. The first aspect involves the manners of thread organization on the GPU. General works for image processing must assign specific computational tasks for all pixels on the image, which are inherently planar, so the 2D thread organization is further suitable. Assimilation for all pixels on the RS image was not required to obtain the rice growth conditions in our study area but not for all rice pixels. We extracted all rice pixels and input rice LAI in one RS image into a 1D vector. Hence, we adopted a 1D manner to organize all threads on the GPU. Second, the model calculations of each thread in this work are considerably more complex than those in other image processing works. As discussed in Section 3, the kernel function PSO_WOFOST consists of numerous intermediate variables, floating-point calculations, iterations and judgment statements, which prevent the speedup of the assimilating progress. We simplified the PSO_WOFOST as much as possible, for instance, removing the unnecessary variables and calculations in the WOFOST model. However, the execution of WOFOST and the PSO algorithm is complex and time-consuming. The optimization and acceleration of each rice pixel's assimilating algorithm still require further work.

The parallel implementation of assimilation can be optimized in numerous aspects in the future. For example, on the basis of different usages of variables, the most applicable memory space is allocated on the GPU to store variables, such as constant, shared and local memories, to improve the parallel program's performance. In addition, CUDA provides a series of accelerated libraries to improve the parallel program's performance, for example, cuBLAS contains all interfaces of functions in the linear algebra BLAS library and cuRAND includes the methods of quickly generating random numbers. The utilization of CUDA - accelerated libraries will greatly improve the parallel program's performance.

Actually, this article does not solve the upscaling problem of the WOFOST model applicated in large-scale. On the

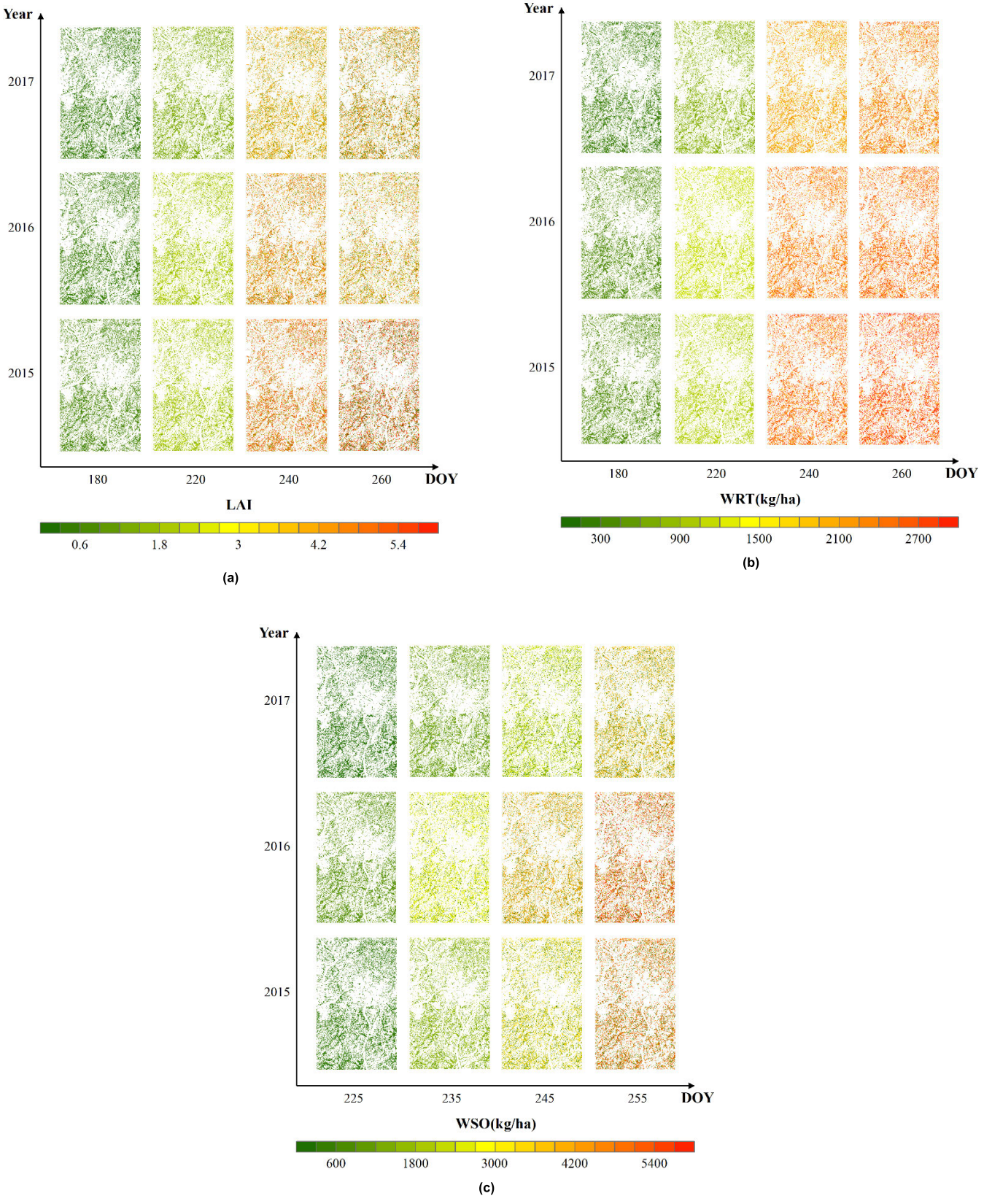

FIGURE 6. Spatial distribution of rice LAI (a), WRT (b) and WSO (c) during the growth period of the entire study area.

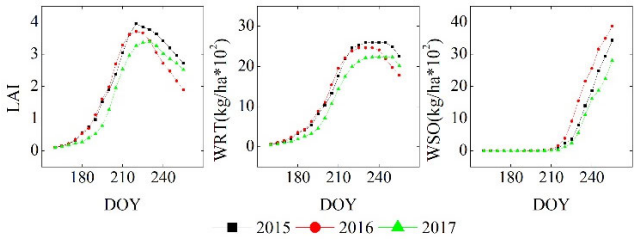

FIGURE 7. Dynamic changes of LAI and WRT in the entire study area. The time step is 5 days. These values are the averages of the entire area at each period.

one hand, when the study area continues to expand, it is completely insufficient to use the data from one meteorological station to represent the entire area due to the spatial heterogeneity. The possible methods for upscaling to a larger area include using grid meteorological data as the model's inputs, conducting spatial interpolation using the data from multiple weather stations. For the issue of meteorological data upscaling, we will continue to study in the future. On the other hand, when the study area continues to expand, due to regional differences in crop growth, the crop parameters in the WOFOST model also need to be adjusted. How to adjust us will also be one important research direction in the future.

VI. CONCLUSION

A highly efficient parallel method based on the GPU with the CUDA platform for the assimilation between the RS data set and WOFOST model by using the PSO algorithm was developed. Each rice pixel's assimilating process between MLAI and SLAI through PSO, which is the most time-consuming work, was allocated to one specific thread on the GPU for the parallel implementation of all rice pixels' assimilation tasks in the entire study area. With the assimilating results, we simulated the crop growth parameters quickly to analyze rice growth conditions in a large scale. The remarkable progress of this work is based on ensuring the precision of assimilating results within an acceptable margin of error and dramatically improving the performance of the assimilation process. The execution times of the parallel and serial programs when handling different sizes of rice pixels are compared. Results show that the parallel implementation based on the GPU has considerably improved the speed of the assimilation between the RS data and WOFOST model and the savings scale with the increase in data size. The speedup reaches almost 240 times in this work. With the highly efficient assimilation results, we simulated rice growth parameters quickly and obtained the spatial distribution of rice growth conditions in a large scale.

REFERENCES

[1] M. Li, S. Zhang, L. Wu, X. Lin, P. Chang, G. Danabasoglu, Z. Wei, X. Yu, H. Hu, X. Ma, W. Ma, H. Zhao, D. Jia, X. Liu, K. Mao, Y. Ma, Y. Jiang, X. Wang, G. Liu, and Y. Chen, "An examination of the predictability of tropical cyclone genesis in high-resolution coupled models with dynamically downscaled coupled data assimilation initialization," *Adv. Atmos. Sci.*, vol. 37, no. 9, pp. 939–950, Sep. 2020.

[2] Z. Zhang, M. Tong, J. A. Sippel, A. Mehra, B. Zhang, K. Wu, B. Liu, J. Dong, Z. Ma, H. Winterbottom, W. Wang, L. Zhu, Q. Liu, H.-S. Kim, B. Thomas, D. Sheinin, L. Bi, and V. Tallapragada, "The impact of stochastic physics-based hybrid GSI/EnKF data assimilation on hurricane forecasts using EMC operational hurricane modeling system," *Atmosphere*, vol. 11, no. 8, p. 801, Jul. 2020.

[3] X. Liu, Y. Duan, and Z. Huo, "Development of a coupled atmosphere–ocean typhoon regional assimilation and prediction system for operational typhoon forecasting by the chinese academy of meteorological Sciences—Part I: Experiments of western north pacific typhoons in 2016," *Ocean Dyn.*, vol. 70, no. 9, pp. 1225–1238, Sep. 2020.

[4] J. Wang, L. Zhang, J. Guan, and M. Zhang, "Evaluation of combined satellite and radar data assimilation with POD-4DEnVar method on rainfall forecast," *Appl. Sci.*, vol. 10, no. 16, p. 5493, Aug. 2020.

[5] D. Xu, A. Shu, F. Shen, J. Min, H. Li, and X. Xia, "Impacts of multiple radiance data assimilation on the simulation of typhoon chan-hom," *Atmosphere*, vol. 11, no. 9, p. 957, Sep. 2020.

[6] I. A. Galkin, B. W. Reinisch, A. M. Vesnin, D. Bilitza, S. Fridman, J. B. Habarulema, and O. Veliz, "Assimilation of sparse continuous near Earth weather measurements by NECTAR model morphing," *Space Weather*, vol. 18, no. 11, Nov. 2020, Art. no. e2020SW002463.

[7] D. Upreti, S. Pignatti, S. Pascucci, M. Tolomio, W. Huang, and R. Casa, "Bayesian calibration of the aquacrop-OS model for durum wheat by assimilation of canopy cover retrieved from VENμS satellite data," *Remote Sens.*, vol. 12, no. 16, p. 2666, Aug. 2020.

[8] Z. Zhang, Z. Li, Y. Chen, L. Zhang, and F. Tao, "Improving regional wheat yields estimations by multi-step-assimilating of a crop model with multi-source data," *Agricult. Forest Meteorol.*, vol. 290, Aug. 2020, Art. no. 107993.

[9] F. Lei, W. T. Crow, W. P. Kustas, J. Dong, Y. Yang, K. R. Knipper, M. C. Anderson, F. Gao, C. Notarnicola, F. Greifeneder, L. M. McKee, J. G. Alfieri, C. Hain, and N. Dokoozlian, "Data assimilation of high-resolution thermal and radar remote sensing retrievals for soil moisture monitoring in a drip-irrigated vineyard," *Remote Sens. Environ.*, vol. 239, Mar. 2020, Art. no. 111622.

[10] P. J. Smith, A. S. Lawless, and N. K. Nichols, "The role of cross domain error correlations in strongly coupled 4D Var atmosphere–ocean data assimilation," *Quart. J. Roy. Meteorol. Soc.*, vol. 146, no. 730, pp. 2450–2465, Jul. 2020.

[11] Y. Hisaki, "Intercomparison of assimilated coastal wave data in the northwestern pacific area," *J. Mar. Sci. Eng.*, vol. 8, no. 8, p. 579, Aug. 2020.

[12] S. Zhang, Z. Liu, X. Zhang, X. Wu, and X. Deng, "Coupled data assimilation and parameter estimation in coupled ocean-atmosphere models: A review," *Climate Dyn.*, vol. 54, no. 9, 2020, pp. 5127–5144.

[13] J. Wang, G. Nie, and C. Xue, "Landslide displacement prediction based on time series analysis and data assimilation with hydrological factors," *Arabian J. Geosci.*, vol. 13, no. 12, pp. 1–9, Jun. 2020.

[14] FU, Shiwen, NIE, Suping, LUO, Yong, CHEN, and Xin, "Implications of diurnal variations in Land Surface Temperature to data assimilation using MODIS LST data," *J. Geographical Ences*, vol. v.30, no. 01, pp. 19–37, 2020.

[15] G. S. Dorfschfer, C. A. S. Tanajura, F. B. Costa, and R. C. Santana, "A new approach for estimating salinity in the southwest atlantic and its application in a data assimilation evaluation experiment," *J. Geophys. Res., Oceans*, vol. 125, no. 9, 2020, Art. no. e2020JC016428.

[16] H. Ghorbanidehno, A. Kokkinaki, J. Lee, and E. Darve, "Recent developments in fast and scalable inverse modeling and data assimilation methods in hydrology," *J. Hydrol.*, vol. 591, Dec. 2020, Art. no. 125266.

[17] P. M. Avellaneda, D. L. Ficklin, C. S. Lowry, J. H. Knouft, and D. M. Hall, "Improving hydrological models with the assimilation of crowdsourced data," *Water Resour. Res.*, vol. 56, no. 5, May 2020, Art. no. e2019WR026325.

[18] E. M. Lim, M. M. Solana, C. Pain, Y. K. Guo, and R. Arcucci, "Hybrid data assimilation: An ensemble-variational approach," in *Proc. 15th Int. Conf. Signal-Image Technol. Internet-Based Syst.*, Nov. 2019, pp. 638–640.

[19] H. Pan, Z. Chen, A. de Wit, and J. Ren, "Joint assimilation of leaf area index and soil moisture from Sentinel-1 and Sentinel-2 data into the WOFOST model for winter wheat yield estimation," *Sensors*, vol. 19, no. 14, p. 3161, Jul. 2019.

[20] Z. Chao, N. Liu, P. Zhang, T. Ying, and K. Song, "Estimation methods developing with remote sensing information for energy crop biomass: A comparative review," *Biomass Bioenergy*, vol. 122, pp. 414–425, Mar. 2019.

[21] J. Huang, X. Gao, H. Huang, M. A. Hongyuan, S. U. Wei, and D. Zhu, "Regional winter wheat maturity date prediction based on MODIS and WOFOST model data assimilation," *Trans. Chin. Soc. Agricult. Mach.*, vol. 50, no. 9, pp. 186–193, Aug. 2019.

[22] X. Jin, Z. Li, H. Feng, Z. Ren, and S. Li, "Estimation of maize yield by assimilating biomass and canopy cover derived from hyperspectral data into the AquaCrop model," *Agricult. Water Manage.*, vol. 227, Jan. 2020, Art. no. 105846.

[23] W. Li, X. Gu, E. Wang, H. Chen, G. Ge, and C. Zhang, "Dynamic estimation of summer maize biomass based on parameter adjustment of crop growth model," *Trans. Chin. Soc. Agricult. Eng.*, vol. 35, no. 7, pp. 136–142, Aug. 2019.

[24] B. K. Lahoz and R. Menard, *Data Assimilation*. Berlin, Germany: Springer, 2009.

[25] Z. Cheng, J. Meng, J. Shang, J. Liu, Y. Qiao, B. Qian, Q. Jing, and T. Dong, "Improving soil available nutrient estimation by integrating modified WOFOST model and time-series Earth observations," *IEEE Trans. Geosci. Remote Sens.*, vol. 57, no. 5, pp. 2896–2908, May 2019.

[26] S. Hu, L. Shi, K. Huang, Y. Zha, X. Hu, H. Ye, and Q. Yang, "Improvement of sugarcane crop simulation by SWAP-WOFOST model via data assimilation," *Field Crops Res.*, vol. 232, pp. 49–61, Dec. 2019.

[27] D. Liu, A. K. Mishra, and Z. Yu, "Evaluation of hydroclimatic variables for maize yield estimation using crop model and remotely sensed data assimilation," *Stochastic Environ. Res. Risk Assessment*, vol. 33, no. 7, pp. 1–13, 2019.

[28] J. Huang, "Regional winter wheat yield forecasting based on assimilation of remote sensing data and crop growth model with Ensemble Kalman method," *Trans. Chin. Soc. Agricult. Eng.*, vol. 28, no. 4, pp. 142–148, 2012.

[29] C. A. Diepen, J. Wolf, H. Keulen, and C. Rappoldt, "WOFOST: A simulation model of crop production," *Soil Use Manage.*, vol. 5, no. 1, pp. 16–24, Mar. 1989.

[30] A. Ceglar, R. van der Wijngaart, A. de Wit, R. Lecerf, H. Boogaard, L. Seguini, M. van den Berg, A. Toreti, M. Zampieri, D. Fumagalli, and B. Baruth, "Improving WOFOST model to simulate winter wheat phenology in europe: Evaluation and effects on yield," *Agricult. Syst.*, vol. 168, pp. 168–180, Jan. 2019.

[31] A. de Wit, H. Boogaard, D. Fumagalli, S. Janssen, R. Knapen, D. van Kraalingen, I. Supit, R. van der Wijngaart, and K. van Diepen, "25 years of the WOFOST cropping systems model," *Agricult. Syst.*, vol. 168, pp. 154–167, Jan. 2019.

[32] C. Gilardelli, R. Confalonieri, G. A. Cappelli, and G. Bellocchi, "Sensitivity of WOFOST-based modelling solutions to crop parameters under climate change," *Ecological Model.*, vol. 368, pp. 1–14, Jan. 2018.

[33] G. Burgers, P. Jan van Leeuwen, and G. Evensen, "Analysis scheme in the ensemble Kalman filter," *Monthly Weather Rev.*, vol. 126, no. 6, pp. 1719–1724, Jun. 1998.

[34] A. CAYA, J. SUN, and C. SNYDER, "A comparison between the 4dvar and the ensemble Kalman filter techniques for radar data assimilation," *Monthly Weather Rev.*, vol. 133, no. 11, pp. 3081–3094, 2005.

[35] B. R. Hunt, E. Kalnay, E. J. Kostelich, E. Ott, D. J. Patil, T. Sauer, I. Szunyogh, J. A. Yorke, and A. V. Zimin, "Four-dimensional ensemble Kalman filtering," *Tellus A: Dyn. Meteorol. Oceanogr.*, vol. 56, no. 4, pp. 273–277, Jan. 2004.

[36] B. R. Hunt, E. J. Kostelich, and I. Szunyogh, "Efficient data assimilation for spatiotemporal chaos: A local ensemble transform Kalman filter," *Phys. D, Nonlinear Phenomena*, vol. 230, nos. 1–2, pp. 112–126, Jun. 2007.

[37] M. Jin, X. Liu, L. Wu, and M. Liu, "An improved assimilation method with stress factors incorporated in the WOFOST model for the efficient assessment of heavy metal stress levels in rice," *Int. J. Appl. Earth Observ. Geoinfor.*, vol. 41, pp. 118–129, Sep. 2015.

[38] A. Ahmadian, A. Elkamel, and A. Mazouz, "An improved hybrid particle swarm optimization and Tabu search algorithm for expansion planning of large dimension electric distribution network," *Energies*, vol. 12, no. 16, p. 3052, 2019.

[39] N. K. Jain, U. Nangia, and J. Jain, "A review of particle swarm optimization," *J. Inst. Eng.*, vol. 99, no. 4, pp. 1–5, 2018.

[40] H. Jing, Z. Tao, G. Yang, Y. Hu, and Y. University, "Particle swarm optimization algorithm for multi-objective programming problems based on elite strategy," *J. Yangtze Univ.*, vol. 15, no. 13, pp. 1–7, Aug. 2018.

[41] J. Kennedy and R. Eberhart, "Particle swarm optimization," in *Proc. IEEE ICNN*, Nov./Dec. 1995, vol. 4, pp. 1942–1948.

[42] C. J. Lin and Y. T. Prasetyo, "A metaheuristic-based approach to optimizing color design for military camouflage using particle swarm optimization," *Color Res. Appl.*, vol. 44, no. 5, pp. 740–748, 2019.

[43] A. Berger, G. Ettlin, C. Quincke, and P. Rodríguez-Bocca, "Predicting the normalized difference vegetation index (NDVI) by training a crop growth model with historical data," *Comput. Electron. Agricult.*, vol. 161, pp. 305–311, Jun. 2019.

[44] A. Hastings, J. CLIFTON-BROWN, M. Wattenbach, C. P. Mitchell, and P. Smith, "The development of MISCANFOR, a new Miscanthuscrop growth model: Towards more robust yield predictions under different climatic and soil conditions," *GCB Bioenergy*, vol. 1, no. 2, pp. 154–170, Apr. 2009.

[45] R. K. Jha, P. K. Kalita, and R. Jat, "Development of production management strategies for a long-duration rice variety: Rajendra Mahsuri—Using crop growth model, DSSAT, for the state of bihar, india," *Paddy Water Environ.*, vol. 18, no. 3, pp. 531–545, Jul. 2020.

[46] X. Mo, S. Liu, Z. Lin, Y. Xu, Y. Xiang, and T. R. McVicar, "Prediction of crop yield, water consumption and water use efficiency with a SVAT-crop growth model using remotely sensed data on the north China plain," *Ecol. Model.*, vol. 183, nos. 2–3, pp. 301–322, Apr. 2005.

[47] J. R. Williams, C. A. Jones, J. R. Kiniry, and D. A. Spanel, "The EPIC crop growth model," *Trans. Asae*, vol. 32, no. 2, pp. 497–511, 1989.

[48] L. Wu, X. Liu, P. Wang, B. Zhou, M. Liu, and X. Li, "The assimilation of spectral sensing and the WOFOST model for the dynamic simulation of cadmium accumulation in rice tissues," *Int. J. Appl. Earth Observ. Geoinfor.*, vol. 25, pp. 66–75, Dec. 2013.

[49] A. Hamamci, "Cellular automata tractography: Fast geodesic diffusion MR tractography and connectivity based segmentation on the GPU," *Neuroinformatics*, vol. 18, no. 1, pp. 25–41, Jan. 2020.

[50] F. Hegedås, K. Klapcsik, W. Lauterborn, U. Parlitz, and R. Mettin, "GPU accelerated study of a dual-frequency driven single bubble in a 6-dimensional parameter space: The active cavitation threshold," *Ultrason. Sonochem.*, vol. 67, Oct. 2020, Art. no. 105067.

[51] Y. Lai, M. Tsai, Z. Tian, N. Qin, C. Yan, S. Hung, Y. Chi, and X. Jia, "A new open source GPU based microscopic Monte Carlo simulation tool for the calculations of DNA damages caused by ionizing radiation—Part II: Sensitivity and uncertainty analysis," *Med. Phys.*, vol. 47, no. 4, pp. 1971–1982, Apr. 2020.

[52] T. Suzuki, S.-Y. Kim, J.-I. Kani, and J. Terada, "Real-time implementation of coherent receiver DSP adopting stream split assignment on GPU for flexible optical access systems," *J. Lightw. Technol.*, vol. 38, no. 3, pp. 668–675, Feb. 1, 2020.

[53] S. Wang, C. Wang, Y. Cai, and G. Li, "A novel parallel finite element procedure for nonlinear dynamic problems using GPU and mixed-precision algorithm," *Eng. Computations*, vol. 37, no. 6, pp. 2193–2211, Feb. 2020.

[54] Z. Wang, L. Cheng, H. Wang, W. Zhao, and X. Song, "Energy optimization by software prefetching for task granularity in GPU-based embedded systems," *IEEE Trans. Ind. Electron.*, vol. 67, no. 6, pp. 5120–5131, Jun. 2020.

[55] R. Zheng, Y.-D. Liu, and H. Jin, "Optimizing non-coalesced memory access for irregular applications with GPU computing," *Frontiers Inf. Technol. Electron. Eng.*, vol. 21, no. 9, pp. 1285–1301, Sep. 2020.

[56] L. Acción, F. Argáello, and D. B. Heras, "Extended anisotropic diffusion profiles in GPU for hyperspectral imagery," *IEEE J. Sel. Topics Appl. Earth Observ. Remote Sens.*, vol. 12, no. 12, pp. 4964–4976, Jul. 2020.

[57] P. G. Bascoy, P. Quesada-Barriuso, D. B. Heras, F. Argáello, B. Demir, and L. Bruzzone, "Extended attribute profiles on GPU applied to hyperspectral image classification," *J. Supercomput.*, vol. 75, no. 3, pp. 1565–1579, Mar. 2019.

[58] L. Javier, H. Dora B, A. Francisco, and D. Mauro, "GPU framework for change detection in multitemporal hyperspectral images," *Int. J. Parallel Program.*, vol. 47, no. 2, pp. 272–292, 2019.

[59] M. A. Hossam, H. M. Ebied, M. H. Abdel-Aziz, and M. F. Tolba, "Accelerated hyperspectral image recursive hierarchical segmentation using GPUs, multicore CPUs, and hybrid CPU/GPU cluster," *J. Real-Time Image Process.*, vol. 14, no. 2, pp. 413–432, Feb. 2018.

[60] J. Liu, Y. Xue, K. Ren, J. Song, C. Windmill, and P. Merritt, "High-performance time-series quantitative retrieval from satellite images on a GPU cluster," *IEEE J. Sel. Topics Appl. Earth Observ. Remote Sens.*, vol. 12, no. 8, pp. 2810–2821, Aug. 2019.

[61] S. Wang, Y. Guan, and L. Shao, "Multi-granularity canonical appearance pooling for remote sensing scene classification," *IEEE Trans. Image Process.*, vol. 29, pp. 5396–5407, 2020.
[62] A. Yusuf and S. Alawneh, "A survey of GPU implementations for hyperspectral image classification in remote sensing," *Can. J. Remote Sens.*, vol. 44, no. 5, pp. 532–550, 2019.
[63] S. C. Wei and B. Huang, "A GPU-accelerated extended Kalman filter," *Proc. SPIE Int. Soc. Opt. Eng.*, vol. 8183, no. 2, pp. 187–193, 2011.
[64] T. Blattner and S. Yang, "Performance study on CUDA GPUs for parallelizing the local ensemble transformed Kalman filter algorithm," *Concurrency Comput., Pract. Exper.*, vol. 24, no. 2, pp. 167–177, Feb. 2012.
[65] F. Zheng, X. Xu, D. Xiang, Z. Wang, and M. Xu, "GPU-based parallel researches on RRTM module of GRAPES numerical prediction system," *J. Comput.*, vol. 8, no. 3, Mar. 2013.
[66] J. Zhao, J. Li, Q. Liu, W. Fan, B. Zhong, S. Wu, L. Yang, Y. Zeng, B. Xu, and G. Yin, "Leaf area index retrieval combining HJ1/CCD and Landsat8/OLI data in the heihe river basin, China," *Remote Sens.*, vol. 7, no. 6, pp. 6862–6885, May 2015.
[67] Z. Qu, H. Li, Y. Wang, J. Zhang, and Y. Yao, "Detection of electricity theft behavior based on improved synthetic minority oversampling technique and random forest classifier," *Energies*, vol. 13, no. 8, p. 2039, 2020.
[68] A. Paul, D. P. Mukherjee, P. Das, A. Gangopadhyay, A. Rao Chintha, and S. Kundu, "Improved random forest for classification," *IEEE Trans. Image Process.*, vol. 27, no. 8, pp. 4012–4024, Aug. 2018.
[69] L. Breiman, "Random forest," *Mach. Learn.*, vol. 45, no. 1, pp. 5–32, 2001.
[70] Z. Xu, X. Huang, L. Lin, Q. Wang, J. Liu, K. Yu, and C. Chen, "BP neural networks and random forest models to detect damage by dendrolimus punctatus walker," *J. Forestry Res.*, vol. 31, no. 1, pp. 107–121, Feb. 2020.
[71] G. Zhou, X. Liu, S. Zhao, M. Liu, and L. Wu, "Estimating FAPAR of rice growth period using radiation transfer model coupled with the WOFOST model for analyzing heavy metal stress," *Remote Sens.*, vol. 9, no. 5, p. 424, Apr. 2017.
[72] S. Wu, J. Huang, X. Liu, J. Fan, and J. Zou, "Assimilating MODIS-LAI into crop growth model with EnKF to predict regional crop yield," in *Computer and Computing Technologies in Agriculture*, vol. 370. 2012, pp. 410–418.
[73] M. Yuping, H. Yingyu, and Z. Liwei, "Study on winter wheat regional simulation model based on remote sensing data and it's simulations in north China," *Acta Meteorol. Sinica*, vol. 44, no. 5, pp. 532–550, 2005.
[74] *Whitepaper NVIDIA Tesla P100: The Most Adavanced Datacenter Accelerator Ever Built Featuring Pascal GP100, the World's Fastest GPU*, NVIDIA, Santa Clara, CA, USA, 2016.
[75] J. Sanders, and E. Kandrot, *CUDA by Example: An Introduction to General-Purpose GPU Programming* Reading, MA, USA: Addison-Wesley, 2010.

BINGYU ZHAO received the B.S. degree in geographic information system from Southwest Jiaotong University, China, in 2016, and the M.S. degree in surveying and mapping engineering from the China University of Geosciences, Beijing, China, in 2019. He is currently pursuing the Ph.D. degree in cartography and geographic information engineering with Beijing Normal University, China.

His research interests include data assimilation, crop growth model, and drought.

MEILING LIU received the B.S. degree in geography from Hunan Normal University, Changsha, China, in 2002, and the M.S. degree in geological remote sensing and the Ph.D. degree in remote sensing of resources and environment from the China University of Geosciences, Beijing, China, in 2006 and 2011, respectively.

She is currently an Associate Professor with the School of Information Engineering, China University of Geosciences. Her research interests include ecosystem modeling, environment, and vegetation by remote sensing.

JIANJUN WU received the Ph.D. degree in cartography and geography information system from the Institute of Geographic Sciences and Natural Resources Research, Chinese Academy of Sciences, Beijing, China, in 2003.

He is currently a Professor with the Faculty of Geographical Science, Beijing Normal University, Beijing. His research interests include disaster risk management, remote sensing, and geographic information systems (GISs).

XIANGNAN LIU received the B.S. degree in geography from Hunan Normal University, Changsha, China, in 1987, and the M.S. and Ph.D. degrees in remote sensing and geographic information system from Northeast Normal University, in 1990 and 1996, respectively.

In 1990, he joined the Faculty of Northeast Normal University. Since 2006, he has been a Professor with the School of Information Engineering, China University of Geosciences, Beijing, China. He is the author of four books and more than 100 articles. His research interests include modeling, quantitative analysis of natural resources, ecological, and environmental systems by remote sensing, GIS, and geostatistics.

MENGXUE LIU received the B.S. degree in geographic information system from the Anhui University of Science and Technology, Huainan, China, in 2016, and the M.S. degree in surveying science and technology from the China University of Geosciences, Beijing, China, in 2019. She is currently pursuing the Ph.D. degree in cartography and geographic information engineering with Beijing Normal University, China.

Her research interests include spatio-temporal fusion of remote sensing data and ecological service.

LING WU received the B.S. degree in geographic information system and the M.S. and Ph.D. degrees in cartography and geographic information engineering from the China University of Geosciences, Beijing, China, in 2007, 2010, and 2013, respectively.

He was a Postdoctoral Researcher with the Institute of Remote Sensing and GIS, Peking University, from 2013 to 2016. He is currently a Lecturer with the School of Information Engineering, China University of Geosciences. His research interests include data assimilation and scale transformation of remote sensing products.